ELSEVIER

Journal of Chromatography A, 796 (1998) 141–156

JOURNAL OF CHROMATOGRAPHY A

Importance of heat of adsorption in modeling protein equilibria for overloaded chromatography

Poonam Raje, Neville G. Pinto*

Department of Chemical Engineering, University of Cincinnati, Cincinnati, OH 45221-0171, USA

Abstract

The heat of adsorption and its dependence on surface coverage has been measured calorimetrically for protein ion-exchange systems of bovine serum albumin and ovalbumin on an anion-exchanger. Experimental data show that protein adsorption is endothermic for both systems which suggests that the process is entropically driven. Also, heat of adsorption decreased with coverage indicating repulsive lateral interactions between adsorbed proteins. The protein adsorption isotherms were modeled with the nonideal surface solution model. This analysis revealed that it is essential to include the entropic contribution in modeling equilibrium behavior. An empirical method for incorporating this effect has been presented.

Keywords: Adsorption isotherms; Nonideal solution model; Proteins; Albumin; Ovalbumin

1. Introduction

High-performance ion-exchange chromatography (HPIEC) is widely employed for the preparative purification of biomolecules [1]. In contrast to analytical operations, in which a linear equilibrium description is adequate, the nonlinear isotherm region is invariably important for overloaded chromatography. The lack of an appropriate model to adequately describe nonlinear equilibria has significantly impeded the design and optimization of preparative chromatography.

The stoichiometric displacement model (SDM) of Regnier and coworkers is a simple and intuitively appealing description of the process of protein ion-exchange. It was originally proposed to describe protein retention in linear ion-exchange chromatography [2,3], and later applied to overloaded protein chromatography [4,5]. This approach models the process of protein adsorption on ion-exchange materials as a stoichiometric reaction described by the mass-action principle. It assumes that ion-exchange is the only mechanism for adsorption, the entire ion-exchange capacity is available to the protein for adsorption, and the surface and mobile phases are thermodynamically ideal. Though SDM is accurate for low protein loadings, it greatly overpredicts adsorption at higher loadings. This indicates that other effects, apart from ion-exchange, are significant at higher loadings.

The steric mass action model (SMA) proposed by Brooks and Cramer in 1992 [6] uses the framework of SDM, and explicitly accounts for the steric hindrance of salt counterions upon protein binding in multicomponent equilibria. The concentration of hindered salt ions is related to the protein surface concentration through the steric factor σ, which is assumed constant for each protein. This model

*Corresponding author.

0021-9673/98/$19.00
PII S0021-9673(97)01071-6

proposes that steric effects primarily limit protein adsorption at high concentrations.

The nonideal surface solution (NISS) model proposed by Li and Pinto in 1994 [7] is a thermodynamically consistent equilibrium model also based on the SDM. The adsorbed phase is modeled as a nonideal surface solution in equilibrium with a nonideal bulk liquid. Nonidealities are characterized by surface and liquid activity coefficients. In the liquid phase, the major source of nonideal behavior is assumed to be interactions between modulator ions, while nonideal surface behavior is assumed to be dominated by nearest neighbor interactions between adsorbed molecules. In contrast to SMA, the NISS model proposes that nonideal surface interactions primarily limit protein adsorption.

Previously [8], we have combined the SMA and NISS models to gain insight into which of these effects actually limit protein adsorption. It was concluded that adsorption isotherm data, by itself, are incapable of revealing which of the two effects, steric hindrance or nonideal surface interactions, govern protein adsorption at high loadings. Hence an independent measurement of at least one effect is needed to obtain a better understanding of protein adsorption.

In this paper we report experimental findings on the nature and magnitude of nonidealities on the surface, for protein ion-exchange. Analysis of these data within the framework of the NISS model, and comparison with independently measured isotherms provide new insights into the main effects that govern protein adsorption.

2. Theory

2.1. NISS model

The NISS model of Li and Pinto [7] is based on the following major assumptions:

1. Competitive binding in ion-exchange systems can be represented by mass-action equilibrium where electroneutrality on the stationary phase is maintained;
2. The effect of the co-ion can be neglected in the ion-exchange process [5,9];
3. The multipointed nature of protein binding can be represented by an experimentally determined characteristic charge [5];
4. Nonideal effects such as aggregation and change in the tertiary structure of the protein are negligible; and
5. Entropic effects are negligible

The adsorption of $n-1$ macromolecules, 1,2,...$n-1$, is considered in the presence of a small counterion (salt), n, called the modulator. The equilibrium description of the system is given by:

$$\begin{aligned} c_1 + \frac{z_1}{z_n} n_n &\Leftrightarrow n_1 + \frac{z_1}{z_n} c_n \\ c_2 + \frac{z_2}{z_n} n_n &\Leftrightarrow n_2 + \frac{z_2}{z_n} c_n \\ &\vdots \qquad\qquad \vdots \\ c_{n-1} + \frac{z_{n-1}}{z_n} n_n &\Leftrightarrow n_{n-1} + \frac{z_{n-1}}{z_n} c_n \end{aligned} \tag{1}$$

where c_i and n_i are, respectively, the bulk and surface concentrations of species i.

For ion-exchange reactions, the equilibrium constants are related to the species activities (a_i) by:

$$K_{ni} = \frac{a_i^s}{a_i}\left(\frac{a_n}{a_n^s}\right)^{\frac{z_i}{z_n}} \quad i = 1.....n-1 \tag{2}$$

In the adsorbed phase,

$$\begin{aligned} a_i^s &= \frac{\gamma_i^s x_i z_i}{z_r} \quad i = 1.....n-1 \\ a_n^s &= \frac{\gamma_n^s x_n z_n}{z_r} \end{aligned} \tag{3}$$

where x_i is the surface mole fraction, z_i is the charge number, γ_i^s is the surface activity coefficient of species i, and z_r is the charge number of the resin.

In the mobile phase,

$$\begin{aligned} a_i &= c_i \quad i = 1.....n-1 \\ a_n &= \gamma_n c_n \end{aligned} \tag{4}$$

Eq. (3) assumes that the standard state for the adsorbed species corresponds to complete saturation of the ion-exchange capacity by the species. The maximum surface concentration possible for any species i is λ/z_i mmol/kg resin. In this state there is no other competing species on the surface, making it

an ideal state (surface activity coefficient is unity). In Eq. (4) it is assumed that the solution activity coefficient of protein is unity, since the molar concentration of proteins is generally small. The standard state for the mobile phase salt (modulator) is assumed to be the hypothetical state if the solute obeyed Henry's law all the way to 1 m*M*. Substituting Eqs. (3) and (4) in Eq. (2),

$$K_{ni} = \frac{\gamma_i^s z_i x_i}{z_r c_i} \left(\frac{\gamma_n c_n z_r}{\gamma_n^s z_n x_n} \right)^{\frac{z_i}{z_n}} \quad i = 1....n-1 \tag{5}$$

Also, by definition, the total ion-exchange capacity of the adsorbent is:

$$\lambda = \sum_{i=1}^{n} (z_i n_i) \tag{6}$$

Thus, it follows that:

$$Z_r = \sum_{i=1}^{n} (z_i x_i)$$

since λ / z_r is the molar ion-exchange capacity of the resin, and $x_i = n_i / (\lambda / z_r)$ is the surface mole fraction of the adsorbed component.

Eqs. (5) and (6) in conjunction with appropriate equations for the activity coefficients in the surface phase and for the modulator in the liquid phase constitute the NISS equilibrium model.

2.1.1. Surface activity coefficients

Surface nonidealities, represented in terms of surface molar excess gibbs energy, can be attributed to the following:

$$G^E = G^E_{\text{electrostatic}} + G^E_{\text{dispersive}} + G^E_{\text{entropic}} \tag{7}$$

where $G^E_{\text{electrostatic}}$ accounts for nonidealities due to long-range electrostatic interactions between adsorbed molecules, $G^E_{\text{dispersive}}$ accounts for nonidealities due to short-range van-der-Waals interactions between the adsorbed species, and G^E_{entropy} is the entropic contribution to nonideality. The short (dispersive) and long-range (electrostatic) interactions, can be lumped as the enthalpic contribution to nonideality G^E_{enthalpy}.

Therefore,

$$G^E = G^E_{\text{enthalpy}} + G^E_{\text{entropy}} \tag{8}$$

Correspondingly,

$$\ln \gamma^s = \ln \gamma^s_{\text{enthalpy}} + \ln \gamma^s_{\text{entropy}} \tag{9}$$

There is no model available for determining the entropic contribution to nonideality, $\gamma^s_{\text{entropy}}$, for the surface phase for protein ion-exchange. Moreover, the models available for the liquid phase cannot be directly incorporated for the surface phase, as they do not meet thermodynamic constraints unique to the surface phase. This has been discussed in detail elsewhere [7].

Though no appropriate model is available for $\gamma^s_{\text{entropy}}$, Talu and Zweibel [10] have successfully adapted the UNIQUAC model to account for surface nonideality due to nearest neighbor interactions. In the present work, this model has been employed in order to obtain a first approximation of enthalpic contributions to nonideality, though it is recognized that the presence of long-range interactions originating from electrostatic forces must be incorporated in a more rigorous approach.

According to Talu's model, the enthalpic contribution to nonideality for the surface phase, $\ln \gamma^s_{\text{enthalpy}}$, is given by:

$$\ln \gamma^s_{\text{enthalpy}} = -S_i \ln \left(\sum_{j=i}^{n} \omega_j \alpha_{ji} \right) + S_i - S_i \sum_{j=i}^{n} \frac{\omega_j \alpha_{ij}}{\sum_{k=i}^{n} \omega_k \alpha_{kj}} \quad i = 1.....n \tag{10}$$

where S_i is the adsorbate shape factor, and ω_i is the surface fraction defined as:

$$\omega_j = \frac{S_j x_j}{\sum_{k=1}^{n} S_k x_k} \tag{11}$$

α_{ij} is the Boltzmann weighting factor for local compositions. It is calculated using Wilson's method [11] for incorporating differences in intermolecular forces between components of the adsorbed phase. α_{ij} is related to the average lateral interaction energy between segments of nearest-neighbor molecules by:

$$\alpha_{ij} = \exp \left[-\frac{C}{2kT} (e_{ij} - e_{jj}) \right] \tag{12}$$

where C is the coordination number for the adsorbed

segments. The energy of interaction parameters e_{ij} and e_{jj} are functions of the spreading pressure. Talu and Zweibel [10] showed that at low temperatures e_{jj} can be calculated from pure component isosteric heat of adsorption data:

$$e_{jj} = \frac{q_{j\pi} - q_{j0}}{\frac{C}{2}NS_j} \quad (13)$$

where $q_{j\pi}$ is the isosteric heat of adsorption of pure j at the same spreading pressure as the mixture, and q_{j0} is the isosteric heat of adsorption at zero spreading pressure. The cross-energy parameters are calculated from:

$$e_{ij} = (e_{ii}e_{jj})^{1/2}(1 - \beta_{ij}) \quad (14)$$

where β_{ij} is an empirical factor that accounts for differences in size and adsorptive properties of the molecules.

2.1.2. Modulator activity coefficients

The method developed by Bromley [12] has been found to be effective for modeling the activity coefficient of strong electrolytes up to an ionic strength of about 6 *M*. In terms of the ionic strength (I) of the liquid, the Bromley equation is expressed as:

$$\ln \gamma_n = \frac{-0.511\sqrt{I}|z_+z_-|}{1+\sqrt{I}} + \frac{(0.06 + 0.6B|z_+z_-|I}{\left(1 + \frac{1.5}{|z_+z_-|}I\right)^2} + BI \quad (15)$$

This equation contains a single coefficient B, which is readily available for all salts commonly used as modulators in protein ion-exchange chromatography.

3. Experimental

3.1. Materials and apparatus

Bovine serum albumin (BSA, pI=4.9, M_r= 69 000, fraction V), ovalbumin (pI=4.7, M_r= 43 500, Grade VII) and imidazole were obtained from Sigma (St. Louis, MO, USA). Matrex PAE-1000 (a weak anion-exchanger, 10- and 50-μm diameter, 1000-Å average pore size, ligand density 360 μequiv./g) was purchased from Amicon (Danvers, MA, USA). It is a silica based, cross-linked polyethylenimine resin with primary, secondary and tertiary amine ligands. Sodium chloride and hydrochloric acid were obtained from Fisher (Fair Lawn, NJ, USA). All reagents were used as received.

Equilibrium studies were carried out in a table top orbital shaker (Model 4518, Forma Scientific, OH, USA). The absorbance measurements were carried out with a UV-160/CL-750 spectrophotometer (Shimadzu, Kyoto, Japan). A Fisher Accumet pH meter (Model 805 MP) was used to measure pH. Columns were packed using a Haskel air driven liquid pump (Alltech, Deerfield, IL, USA). All elutions were performed on an integrated HPLC system, HP1100 (Hewlett-Packard, West Chester, PA, USA).

The heat of adsorption was measured using a Microscal flow microcalorimeter (Gilson, Westerville, OH, USA). The flow microcalorimeter (FMC), shown in Fig. 1, is an instrument designed to measure small thermal changes which occur during adsorption and desorption of molecular species carried in a fluid stream. The FMC operates isothermally and can precisely quantify the heats of sorption, evacuation and wetting. It has a precision fluid delivery system (micropumps and syringes) which can deliver flow-rates in the range 0.33–330 ml/h, a vacuum system to pre-evacuate a sample in situ, a block heater and monitor to control cell temperature, and an analog recorder to monitor experiments. Fluid contact materials are PTFE and KALREZ®. Calibration is via electrical energy dissipation in the cell under static or flowing conditions. FMC instrumentation can link the test cell effluent to an appropriate downstream detector (DSD) so concentration changes can be monitored. Microscal calorimeter digital output and sequencing software (CALDOS) records, calibrates and displays data from both detectors so that enthalpy changes and mass transfer can be quantified. CALDOS can be used with the automatic sequence controller (ASC) to execute predefined experimental events.

3.2. Procedures

3.2.1. Isotherms

BSA and ovalbumin adsorption isotherms were

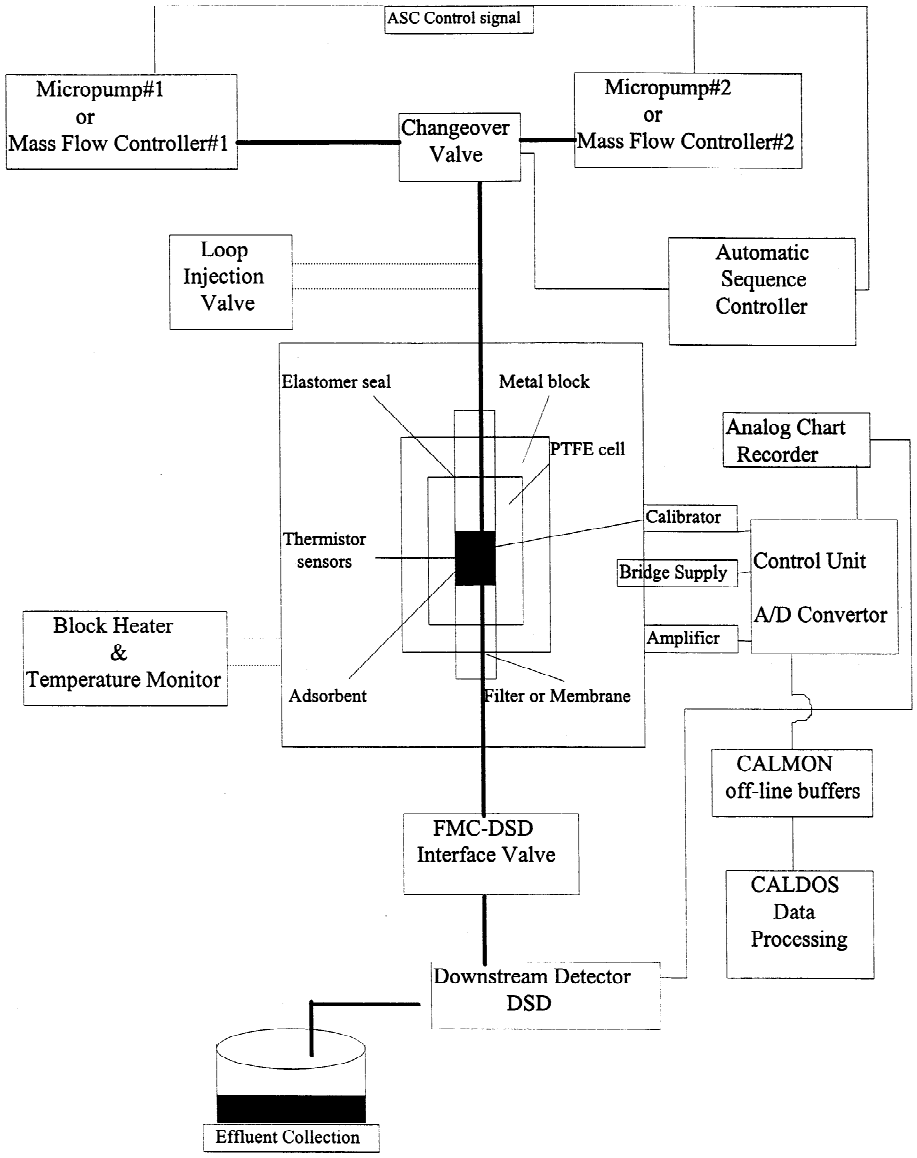

Fig. 1. Schematic of flow microcalorimeter.

measured at selected sodium chloride concentrations in 20 m*M* imidazole buffer at 30°C (pH 7.0) by the batch method. PAE-1000 was first weighed into test-tubes, and protein solution of a known concentration was pipetted into the tube. The test tubes were sealed with parafilm, placed in the shaker, and agitated at 200 rpm for 24 h at 30°C. Preliminary experiments have established that equilibrium can be reached in 8–10 h. After equilibration, the slurry solution was allowed to stand for 1 h before filtering with a 0.45-μm filter. The absorbance of the filtrate was measured at 280 nm to obtain the equilibrium solution concentration. The equilibrium distribution was calculated from a mass balance.

3.2.2. Determination of effective charge (z_i) and equilibrium constant (K_{ni})

The effective charge and the equilibrium constant of the proteins was measured by linear isocratic

elution on a 25×0.46 cm I.D. column for a range of salt concentrations. The column was first washed with 1 *M* salt buffer at a flow-rate of 1.0 ml/min, and the protein retention under these conditions was considered to be the dead time. The column was then equilibrated with 0.02 *M* imidazole buffer (pH 7.0) having the desired salt concentration. Following equilibration, 20 μl of protein solution of concentration 2 mg/ml was injected. The column temperature was maintained at 30°C, and the salt used was sodium chloride. The retention time at each salt concentration was used to find the capacity factor using the equation:

$$k' = \frac{t_R - t_0}{t_0} \tag{16}$$

Subsequently, z and K were calculated using the equation [8]:

$$\ln k' = \ln\left(\frac{K_{n1}\phi\lambda}{z_1}\right) - \frac{z_1}{z_n}\ln(\gamma_n c_n) \tag{17}$$

where γ_n is the activity coefficient correction in the liquid phase for the salt, and was calculated using Eq. (15).

3.2.3. Determination of heat of adsorption

The heat of adsorption experiments started with loading a known weight of the ion-exchange resin (PAE-1000) in a clean and dry flow cell. About 60 mg of 50-μm resin was loaded for each measurement; the 50-μm particle size was chosen because these particles were found to pack more consistently and easily than the 10-μm particles. The cell chamber was maintained at 30°C. The loaded cell was equilibrated with 20 m*M* imidazole buffer (pH 7.0) fed at 3.3 ml/h. Once the bed was in thermal and mass equilibrium with the buffer, a 91-μl pulse of sample (protein or salt solution of known composition) was injected into the flowing buffer stream. Adsorption of sample components on the ion-exchange resin alters the thermal and mass equilibrium in the cell. The temperature change is recorded by the thermistor. Using CALDOS data processing software, with an electrical calibration standard, the temperature time trace was converted to a heat versus time signal, from which the total heat released can be calculated. A typical result is shown in Fig. 2. The amount adsorbed is calculated from a mass balance, by determining the amount of solute in the effluent by UV detection, and subtracting this from the amount fed.

4. Results and discussion

Adsorption isotherms measured for BSA and ovalbumin at 100 m*M* and 200 m*M* sodium chloride concentrations are shown in Figs. 3 and 4. As can be seen, type I isotherms were obtained in all cases and adsorption capacity was found to be very sensitive to salt concentration. z and K, measured by linear isocratic elutions, for the two proteins, are reported in Table 1, along with the range of salt concentrations at which these elutions were carried out. These values compare well with those reported earlier [13]. Both, the isotherms and the elution data indicate that BSA is a more strongly adsorbed protein (higher K) with a higher adsorption capacity than ovalbumin.

The isosteric heat of adsorption (q^{st}) for chloride ion measured at different surface coverages is shown in Fig. 5. It can be seen that the heat of adsorption is independent of coverage and is approximately 0.17 kcal/mol, a magnitude consistent with expectations for ion-exchange of small molecules [14] (1 cal = 4.184 J). The experimental observation that q^{st} does not depend on surface concentration implies that chloride ions already adsorbed on the resin do not influence subsequent chloride adsorption; i.e., there are no significant surface interactions between adsorbed chloride ions.

Fig. 6 shows the isosteric heat of adsorption for BSA and ovalbumin measured at different surface mole fractions. It should be noted that for all surface coverages the heat of adsorption was found to be endothermic for both BSA and ovalbumin. Since the enthalpic contribution to the Gibbs free energy (ΔG) is unfavorable (ΔH is positive), it is clear from Eq. (18) that a favorable contribution from entropy (positive ΔS) is required to make the adsorption energetically feasible.

$$\Delta G = \Delta H - T\Delta S \tag{18}$$

The contribution from entropy can manifest in

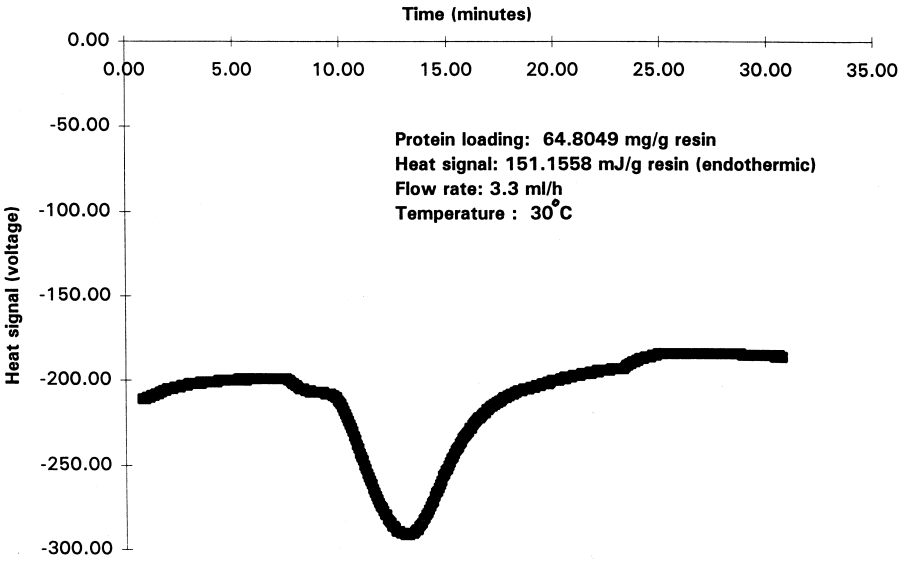

Fig. 2. Typical heat signal from flow microcalorimeter for BSA adsorption on PAE-1000 (50 μm).

different forms: release of counter ions on adsorption, release of water from the protein surface, reorientation of the protein on the surface, conformational changes of the protein, volume exclusion, steric hindrance of ion- exchange groups etc. All of these effects need to be quantified in order to model the adsorption equilibrium effectively. Unfortunately, as was mentioned earlier, there is no thermodynamically consistent model for quantifying entropy changes on the surface. A more detailed discussion on this will be given later.

It is important to note that the conclusion reached

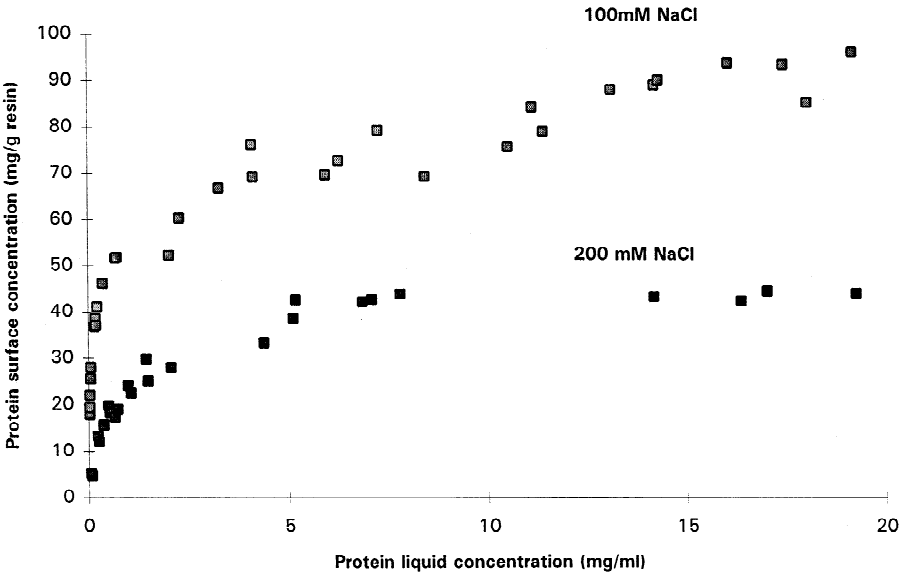

Fig. 3. Adsorption isotherm for BSA at 100 and 200 m*M* NaCl, $T = 30°C$, Resin PAE-1000.

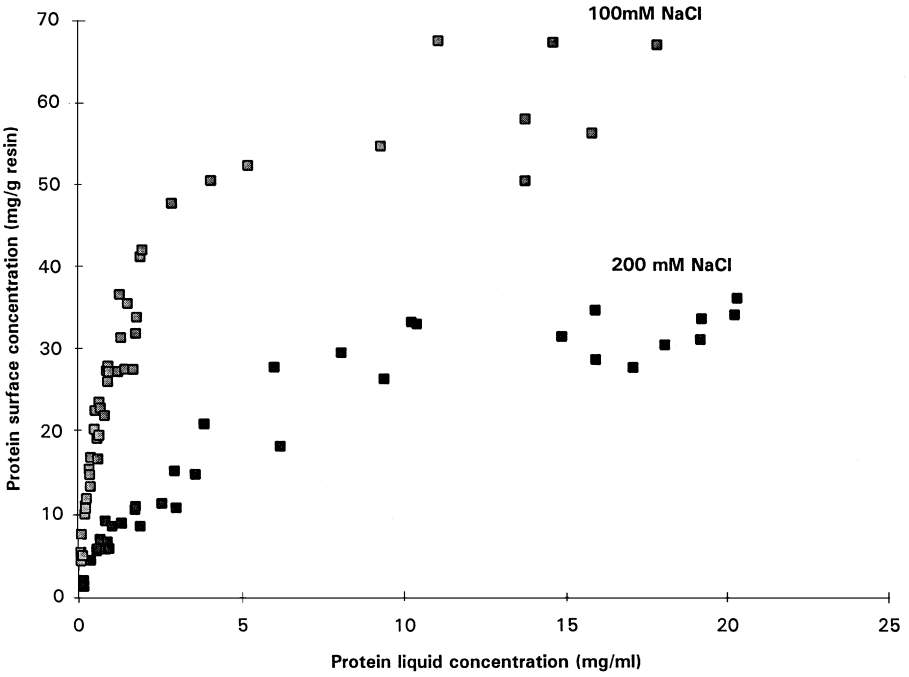

Fig. 4. Adsorption isotherm for ovalbumin at 100 and 200 m*M* NaCl, *T*, 30°C, resin PAE-1000.

with respect to the entropic contribution is specific to the adsorption systems studied; this result cannot be generalized to other protein ion-exchange systems. In fact, Norde [15] has experimentally observed a wide range of behavior of the heat of adsorption with coverage for proteins. This behavior ranged from highly exothermic to endothermic heats of adsorption, with heats increasing, decreasing or remaining constant with coverage.

In contrast to chloride adsorption (Fig. 5), the isosteric heats of adsorption for BSA and ovalbumin are strongly dependent on surface coverage (Fig. 6). This indicates that significant surface interactions are present between adsorbed protein molecules. Fig. 6 also reveals that the heat of adsorption decreases linearly with coverage for both proteins in the range investigated. This decrease suggests repulsive interactions between adsorbed protein molecules.

The experimental enthalpy data for both BSA and ovalbumin were fit to the straight line equation:

$$q_{i\pi}^{st} - q_{i0}^{st} = -mx_i \tag{19}$$

where $q_{i\pi}^{st}$ is the isosteric heat of adsorption at surface mole fraction x_i, and q_{i0}^{st} is the isosteric heat of adsorption at zero coverage. The parameters m and q_{i0}^{st} were found, respectively, from the slope and the intercept of the best-fit line. Since larger repulsive interactions between adsorbed molecules will result in a larger negative slope of the isosteric heat curve, it can be concluded from the values of m for BSA and ovalbumin (Table 2) that repulsive interac-

Table 1
Effective charge (z) and equilibrium constant (K)

Protein	Salt concentration range (m*M*)	Effective charge (z)	Equilibrium constant (K)
BSA	250–350	4.9	$8 \cdot 10^9$
Ovalbumin	130–200	4.2	$6.7 \cdot 10^7$

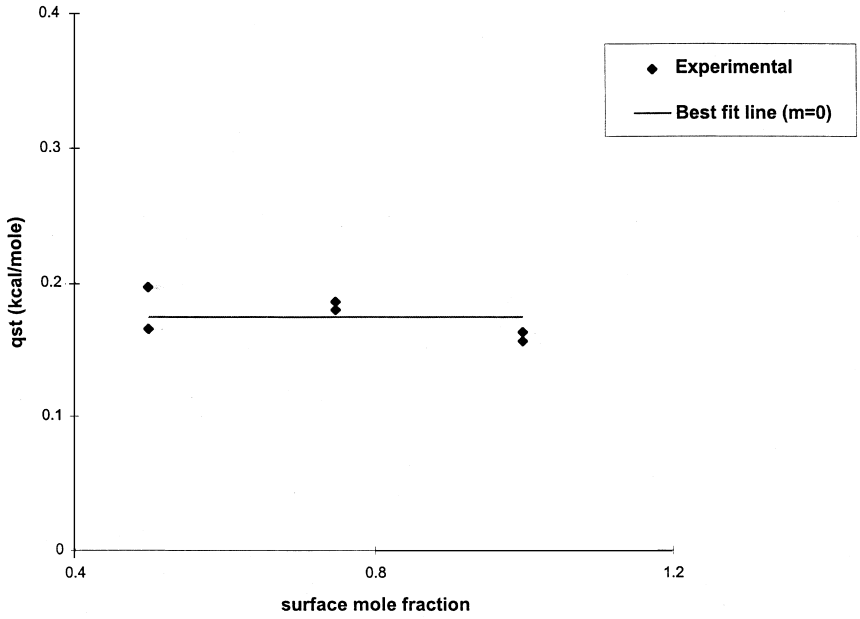

Fig. 5. Dependence of isosteric heat of adsorption on coverage for chloride at 30°C.

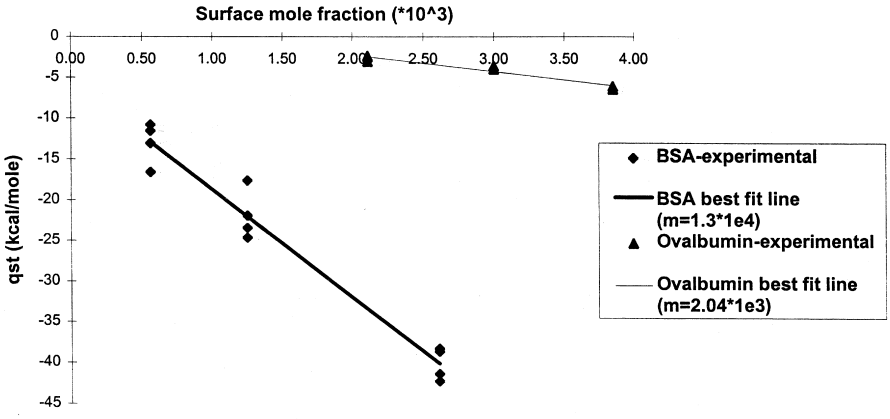

Fig. 6. Dependence of isosteric heat of adsorption on coverage for BSA and ovalbumin at 30°C.

Table 2
Best-fit coefficients for isosteric heat data

Species	m (negative slope)	q_{i0}^{st} (kcal/mol)
BSA	13286.5	−5.46
Ovalbumin	2042.86	1.866
Chloride	0	0.17

tions between adsorbed BSA molecules are higher than those between adsorbed ovalbumin molecules.

4.1. Analysis with the NISS model

In order to obtain additional insight on the entropic contribution to the adsorption of BSA and

ovalbumin, the NISS model described earlier was used. Since this model incorporated only the enthalpic effect, differences between experimental adsorption isotherms and isotherms predicted by NISS will give some indication of the magnitude of the entropic contribution and its dependence on surface coverage.

Use of the NISS model (Eqs. (5), (6) and (10)) requires knowledge of the surface concentration dependence of the isosteric heat of adsorption, $q_{i\pi}^{st} - q_{i0}^{st}$, and the shape factor, S_i, for each species. As described earlier, the isosteric heat data were obtained experimentally (Figs. 5 and 6), and have been characterized using Eq. (19) (Table 2).

The shape factor S_i is defined as the ratio of the free perimeter of the protein molecule to that of a standard molecule [16]. Here the modulator is considered as the standard molecule. The shape factor quantifies the total number of external, lateral contacts of the protein. In this study, molecular dimensions of the protein and the modulator in solution have been used to estimate the shape factor and are reported in Table 3 [17–19]. It should be noted that this approach assumes that the shape of the molecule is not significantly changed by ion-exchange. It is possible that proteins re-orient themselves or change conformation under overloaded conditions, in order to minimize the free energy. In light of such possible conformation and orientation changes, the calculation of shape factor using molecular dimensions in solution is open to question. A more rigorous estimation of shape factor would require data on the conformation of a protein after adsorption, and also on the orientation of the protein as a function of surface concentration. Though such a description is desirable, present methods of imaging adsorbed proteins make these difficult to obtain. Also, sensitivity studies done previously [8] with respect to the shape factor have revealed that in absence of salt–salt lateral interactions the isotherm prediction is only weakly sensitive to the shape factor. Since experimental heat of ion-exchange data for chloride indicates that surface interactions between adsorbed chloride ions are negligible, it is reasonable to calculate the shape factor from the species molecular dimensions in solution.

The shape factor S_i, reported in Table 3, was used to calculate the surface fraction ω_i (Eq. (11)), and the isosteric heat of adsorption dependence on surface coverage (Table 2) was used to estimate the Boltzmann weighing factor α_{ij} (Eqs. (12) and (13)). These were then used to evaluate the enthalpic surface activity coefficient using Eq. (10). Subsequently, the set of nonlinear isotherm Eqs. (5) and (6), which specified the equilibrium constant and electroneutrality constraints, along with the enthalpic surface activity coefficient, were solved with a commercial nonlinear equation solver program using Powell hybrid method [20] to predict the equilibrium surface concentrations for a range of liquid concentrations.

Figs. 7 and 8 depict comparisons of the NISS predictions with the experimental isotherms for BSA at 200 m*M* and 100 m*M* NaCl, respectively. It is clear that the simulated isotherms are greatly underpredicted in all cases. Assuming the validity of Talu's UNIQUAC model for calculating the enthalpic contribution to nonideality, only the entropic contribution to nonideality has been neglected in the NISS model. Thus, the difference between the NISS predictions and the experimental curves in Figs. 7 and 8 is a measure of the magnitude of the entropic driving force for adsorption. Clearly, a large entropic effect is involved in the adsorption of BSA on PAE 1000 in the salt range studied. A similar effect was found for ovalbumin. Protein adsorption systems which are principally entropy driven are not uncommon. Norde [15] shows experimental evidence, through calorimetric measurements, of such entropy governed systems and discusses various factors

Table 3
Molecular characteristics used in estimation of shape factor

Species	Shape of imprint	Dimensions	Shape factor	Ref.
BSA	Equilateral triangle	80 Å (side)	11.51	[17]
Ovalbumin	Ellipse	25.2·50.4 Å (minor·major axis)	11.38	[18]
Chloride	Circle	6.64 Å (hydrated diameter)	1	[19]

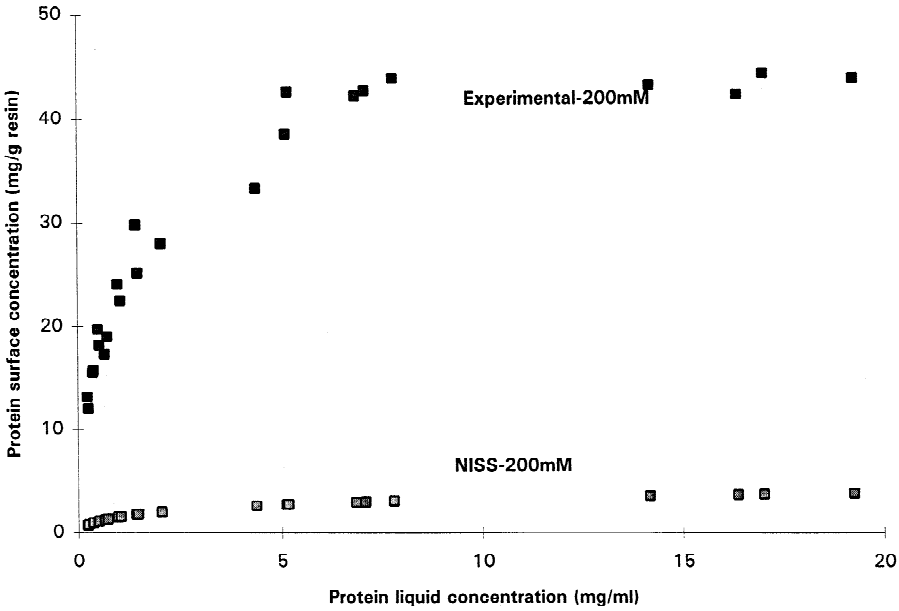

Fig. 7. Comparison of experimental and simulated (NISS) isotherm for BSA at 200 m*M* NaCl.

(enthalpic and entropic) that determine protein adsorption.

In analyzing the data in Figs. 7 and 8, the ratio of NISS predicted to experimental surface concentrations at fixed protein liquid concentrations were calculated. This ratio is plotted in Figs. 9 and 10 for BSA and ovalbumin, respectively. Surprisingly, the ratio was found to be approximately constant for both proteins over the range of liquid concentrations studied. Additionally, this ratio was independent of

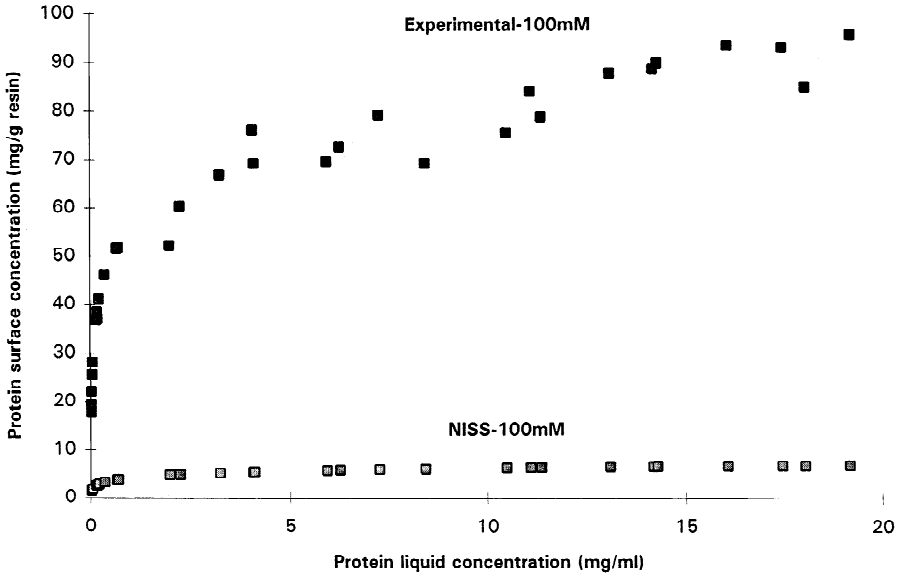

Fig. 8. Comparison of experimental and simulated (NISS) isotherm for BSA at 100 m*M* NaCl.

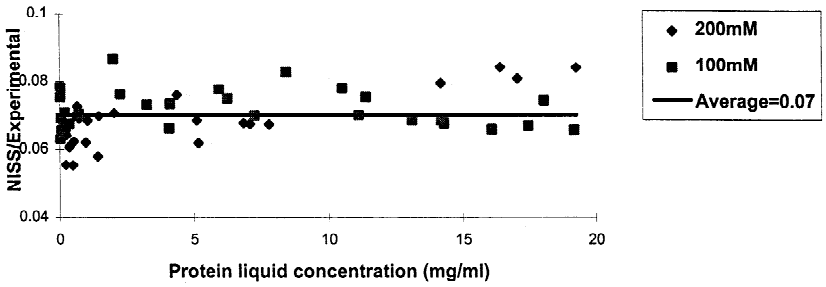

Fig. 9. Ratio of NISS/experimental adsorption as a function of BSA liquid concentration.

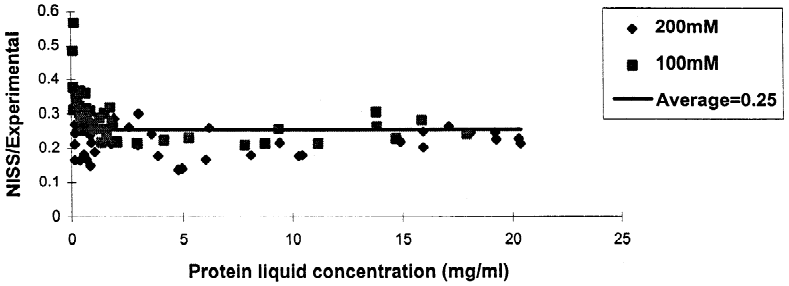

Fig. 10. Ratio of NISS/experimental adsorption as a function of ovalbumin liquid concentration.

the salt concentration. It is recognized that there has to be a protein concentration dependence for this ratio, since at the limit of zero protein concentration the ratio must approach unity. It is suspected that this dependence occurs in the dilute region of the isotherm, where the concentration dependence is very steep; indeed, there is some indication of this with the ovalbumin data (Fig. 10). This implies that for much of the isotherm, and particularly for the nonlinear region that is of importance in overloaded chromatography, the ratio is approximately constant and independent of salt concentration. Thus, in the absence of a rigorous method for calculating the entropic contribution, it should be possible to conveniently quantify the entropic effect by incorporating this ratio into the calculation of the isotherm.

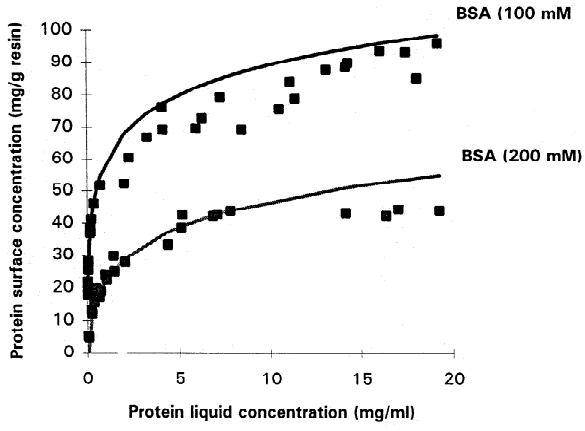

Fig. 11. Experimental and corrected simulated isotherms for BSA at 100 and 200 m*M* NaCl.

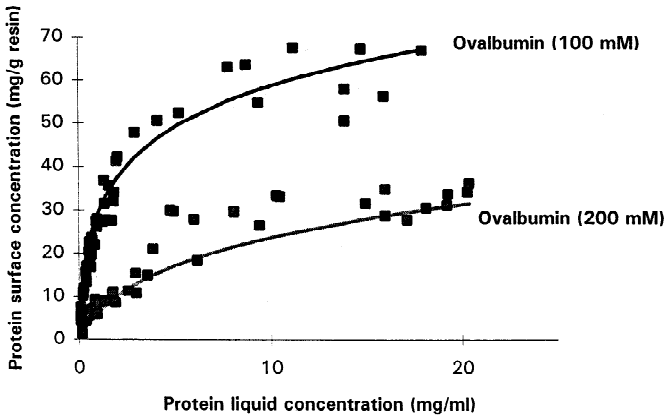

Fig. 12. Experimental and corrected simulated isotherms for ovalbumin at 100 and 200 m*M* NaCl.

Shown in Figs. 11 and 12 are the isotherms calculated for BSA and ovalbumin, respectively, when the constant ratios shown in Figs. 9 and 10 are used with the NISS model. It can be seen that the experimental data are well characterized over the entire range of protein liquid concentration and as a function of salt concentration.

4.2. Qualitative comparison of entropic and enthalpic contribution

The experimental measurement of the isosteric heat of adsorption has revealed the importance and need for incorporating entropic contributions when modeling protein adsorption. As has been shown, the experimental data, when analyzed within the NISS framework, suggest that repulsive interactions reduce adsorption while entropic effects increase adsorption. Since activity coefficients are a measure of these effects, it is useful to make a comparison of the contributions of each of the effects to the overall activity coefficient on the surface. Shown in Fig. 13a is the enthalpic contribution to the surface activity coefficient as a function of surface concentration for BSA, as predicted by the Talu's model (Eq. (10)). It is seen that enthalpic effects give large positive values of $\ln \gamma^{s}_{enthalpy}$, which increase with concentration. These positive values suppress adsorption. It would thus be expected that the entropic contribution to surface activity coefficient would be the opposite; i.e., large negative values of $\ln \gamma^{s}_{entropy}$ that decrease with increasing concentration.

As was mentioned earlier, there are many factors that can contribute to the entropy change accompanying the adsorption of a protein, and there is no model that can quantify the change rigorously. The SMA model by Brooks and Cramer [6] incorporates the entropic effect due to steric hindrance of ion-exchange groups by proteins. However, this entropic effect reduces adsorption by limiting accessible ion-exchange sites for protein adsorption. This is in

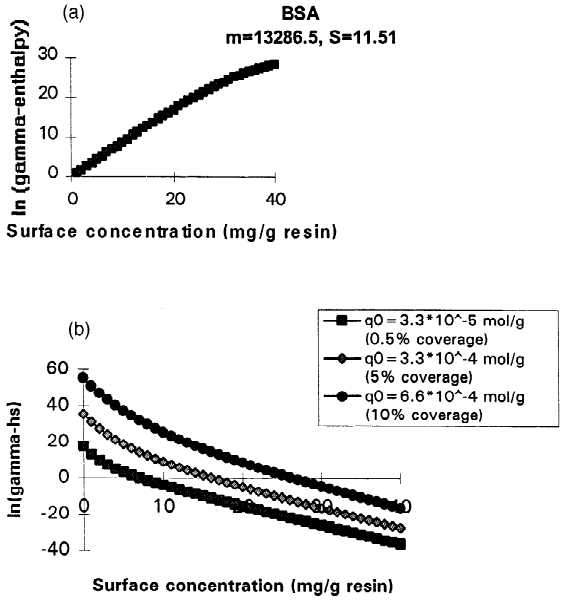

Fig. 13. (a) NISS prediction of enthalpic contribution to surface activity coefficient, (b) hard sphere prediction of entropic contribution to activity coefficient.

contrast to the positive contribution of entropy indicated by the experimental data. In an attempt to establish if entropy can provide the driving force necessary to overcome the effects of enthalpy as manifested in Fig. 13a, a liquid phase model was used as a first approximation for estimating the corresponding effect on the surface phase. Since some of entropic effects, such as entropy of exchange, conformation and orientation changes of the protein on surface are purely surface related, no analogous models could be found for calculating these in the liquid phase. Liquid phase models do however exist for calculating the entropic contribution to nonideality by volume exclusion (hard sphere).

The hard sphere contribution to the Gibbs excess energy (G^{E}_{hs}) has been quantified for ternary liquid solutions by Haynes et al. [21].

$$G^{E}_{hs} = -RT\sum q_i \ln(1-\xi_3) - \frac{RT}{V^{\theta}_0}\sum_{i\neq 0} q_i V^{\theta}_i - \frac{RTV_{ad}}{V^{\theta}_0}(1-\sum_{i\neq 0}\phi_{is})\ln(1-\sum_{i\neq 0}\phi_{is}) + \frac{6kTV_{ad}}{\pi}\left[\frac{3\xi_1\xi_2-\xi_2^3/\xi_3}{(1-\xi_3)} + \frac{\xi_2^3}{\xi_3^2}\ln(1-\xi_3) + \frac{\xi_2^3}{(1-\xi_3)^2}\right] \quad (20)$$

where subscript $i=0$ is for an inert solvent and q_i is the molar quantity of species i.

$$\xi_m = \frac{\pi N_{av}\sum_i q_i d_i^m}{6V_{ad}} \quad m = 1,2 \text{ or } 3$$

and

$$\phi_{is} = \frac{q_i V^{\theta}_i}{V_{ad}}$$

is the volume fraction of species i.

It has been assumed for simplicity that the same equation holds for the adsorbed phase. This approach models the adsorption surface as having a monolayer of proteins and salt ions, with space between salt ions and proteins filled with inert solvent molecules. Using Eq. (20), the surface activity coefficient for species i can be found by:

$$(\ln\gamma^{s}_{hs})_i = \frac{\partial\left(\frac{G^{E}_{hs}}{RT}\right)}{\partial q_i} \quad (21)$$

Thus,

$$(\ln\gamma^{s}_{hs})_i = -\ln(1-\xi_3)\frac{V^{\theta}_1\sum q_i}{V_{ad}(1-\xi_3)} + \frac{V^{\theta}_i}{V^{\theta}_0}\ln\left(1-\sum_{i\neq 0}\phi_{is}\right) + \frac{d_i(1-\xi_3)\left(3\xi_1 d_i + 3\xi_2 - \frac{3\xi_2^3 d_i}{\xi_3} + \frac{d_i^2\xi_2^3}{\xi_3^2}\right) + d_i^3\left[3\xi_1\xi_2 - \frac{\xi_2^3}{\xi_3}\right]}{(1-\xi_3)^2} + d_i^2\ln(1-\xi_3)\left(\frac{3\xi_2^2\xi_3 - 2\xi_2^3 d_i}{\xi_3^3}\right) - \frac{d_i^3\xi_2^3}{\xi_3^2(1-\xi_3)} + d_i^2\left(\frac{3\xi_2^2(1-\xi_3)+2\xi_2^3 d_i}{(1-\xi_3)^3}\right) \quad (22)$$

The use of Eq. (22) to model the hard-sphere contribution to entropy requires the following parameters: A_s, the surface area available for adsorption; V_{ad}, the volume of the adsorbed phase; d_i, the hard sphere diameter for the species; V^{θ}_i, the partial molar volume of the species and q_0, the surface concentration of the inert solvent. A_s was obtained from the manufacturer's literature on the resin, V_{ad} was calculated assuming the thickness of the adsorbed layer is $d_{chloride}+d_{BSA}$. Thus, $V_{ad}=A_s(d_{chloride}+d_{BSA})$. d_i has been reported for BSA, chloride and water [21]. V^{θ}_i was calculated assuming that all the species are spherical molecules with equivalent hard sphere diameters and form ideal solutions. Thus, $V^{\theta}_i=(N_{av}\pi d_i^3/6)q_0$ was calculated assuming w% of resin surface is covered with inert solvent (water) having a spherical imprint of the equivalent hard-sphere diameter. Thus $q_0 = w\%[A_s/(\pi d_0^2/4)N_{av}]$. Simulations were performed at three values of w (0.5, 5 and 10) to study the influence of the solvent.

Fig. 13b shows the predictions from Eq. (22) using the parameters summarized in Table 4. As can be seen, $\ln\gamma^{s}_{hs}$ values are predicted to decrease with increasing protein concentration, as would be required to counter the effect from enthalpy discussed earlier. It is also predicted that the magnitude of $\ln\gamma^{s}_{hs}$ is strongly dependent on the amount of solvent present on the surface. As the amount

Table 4
Simulation parameters for estimation of γ^{s}_{hs} (Fig. 13)

A_s	500 m^2/g
V_{ad}	$3.16 \cdot 10^{-6}$ m^3/g
d_i	
BSA	59.6 Å
Chloride	3.62 Å
Water	4.0 Å
V_i^{Θ}	
BSA	$66731.3 \cdot 10^{-6}$ m^3/mol
Chloride	$14.95 \cdot 10^{-6}$ m^3/mol
Water	$20.17 \cdot 10^{-6}$ m^3/mol
q_0 (w% coverage)	
0.5%	$3.3 \cdot 10^{-5}$ mol/g
5.0%	$3.3 \cdot 10^{-4}$ mol/g
10.0%	$6.6 \cdot 10^{-4}$ mol/g

decreases the magnitude of $\ln \gamma^{s}_{hs}$ decreases, and it is possible to identify conditions at which large negative values for $\ln \gamma^{s}_{hs}$ are obtained, as would be required to counter the contributions of $\ln \gamma^{s}_{enthalpy}$ shown in Fig. 13a.

It must be re-emphasized that the $\ln \gamma^{s}_{hs}$ equation is rigorously applicable only to a bulk phase. Thus, a quantitative comparison with the $\ln \gamma^{s}_{enthalpy}$ from the NISS cannot be made. However, the consistency between the predicted and expected trends is encouraging, and does re-enforce the point that the contribution from entropy can be very significant.

5. Conclusions

Calorimetric measurements of the heat of adsorption for BSA and ovalbumin adsorption on PAE-1000 systems have revealed important information on the nature and magnitude of the nonidealities on the surface for proteins. An endothermic heat of adsorption has shown that the process is entropically driven. Furthermore, the heat of adsorption was found to decrease with surface coverage for proteins, indicating repulsive interactions between adsorbed proteins. It has been shown that incorporation of only enthalpic nonidealities using the NISS model greatly underpredicts the adsorption isotherms; entropic contributions must be incorporated. Though there is no rigorous method for calculating these, for ovalbumin and BSA a simple empirical method for quantifying this effect has been presented.

Symbols

a_i	Bulk activity of i
a^{s}_i	Surface activity of i
B	Bromley's constant
c_i	Bulk concentration (mM)
C	Coordination number for adsorbed segments
d_i	Hard sphere diameters of species i
e_{ij}	Energy of interaction parameter
G^{E}_{hs}	Hard sphere contribution to Gibbs excess energy (J/g)
I	Ionic strength (molal)
k	Boltzmann constant
k'	Elution capacity factor
K_{ni}	Equilibrium constant for ion-exchange of n,i
m	Slope coefficient (Eq. (18))
n	Number of components
n_i	Surface concentration (mmol/kg resin)
n_i^{*}	Equilibrium surface concentration
N	Avogadro number
q_i	Molar concentration of species i on surface (mol/g)
$q_{i\pi}$	Isosteric heat of adsorption at spreading pressure of mixture (kcal/mol)
q_{i0}	Isosteric heat of adsorption at zero spreading pressure
R	Universal gas constant (8.314 J/mol/K)
S	Shape factor
t_0	Dead time (min)
T	Temperature (K)
V_{ad}	Volume of adsorbed layer (m^3/g)
V_i^{θ}	Partial molar volume of species i (m^3/mol)
x_i	Surface mole fraction of i
z_i	Charge number of i
z_r	Charge number of resin
z_+, z_-	Charge on salt cation, anion

Greek symbols

α_{ij}	Boltzmann weighting factor
β_{ij}	Empirical factor accounts for differences in size and adsorptive properties
ΔG	Change in Gibbs free energy (kcal/mol)
ΔH	Change in enthalpy (kcal/mol)

ΔS	Change in entropy (kcal/mol)
ϕ_{is}	Volume fraction of species *i*
γ_i^s	Surface activity coefficient of *i*
γ_{entrop}^s	Enthalpic surface activity coefficient
$\gamma_{entropy}^s$	Entropic surface activity coefficient
λ	Equivalent ion-exchange capacity of resin (mequiv./kg resin)
ω_i	Surface fraction
Subscripts	
0	inert solvent
n	modulator
Superscript	
s	surface phase

References

[1] F.E. Regnier, Science 222 (1983) 245.
[2] W. Kopaciewicz, M.A. Rounds, J. Fausnaugh, F.E. Regnier, J. Chromatogr. 266 (1983) 3.
[3] M.A. Rounds, F.E. Regnier, J. Chromatogr. 283 (1984) 37.
[4] F.E. Regnier, I. Mazsaroff, Biotech. Prog. 3 (1987) 22.
[5] A. Velayudhan, Cs. Horváth, J. Chromatogr. 443 (1988) 13.
[6] C.A. Brooks, S.M. Cramer, AIChE J. 38 (1992) 1969.
[7] Y. Li, N.G. Pinto, J. Chromatogr. A 658 (1994) 445.
[8] P. Raje, N.G. Pinto, J. Chromatogr. A 760 (1997) 89.
[9] R.R. Drager, F.E. Regnier, J. Chromatogr. 359 (1986) 147.
[10] O. Talu, I. Zweibel, AIChe J. 32 (1986) 1263.
[11] G.M. Wilson, J. Am. Chem Soc. 86 (1964) 127.
[12] L.A. Bromley, AIChE J. 19 (1973) 313.
[13] Y. Li, Ph.D. Dissertation, University of Cincinnati, Cincinnati, OH, 1997.
[14] F. Helfferich, Ion Exchange, McGraw Hill, New York, 1962, p. 166.
[15] W. Norde, J. Dispers. Sci. Tech. 13 (1992) 363.
[16] O. Talu, Ph.D. Dissertation, Arizona State University, Tempe, AZ, 1984.
[17] D.C. Carter, J.X. Ho, Advances in Protein Chemistry, Academic Press, New York, Vol. 145, 1994, p. 160.
[18] T. Matsumoto, J. Chiba, J. Chem. Soc. Faraday Trans. 86 (1990) 2877.
[19] M.T.W. Hearn, A.N. Hodder, M.I. Aguilar, J. Chromatogr. 443 (1988) 97.
[20] D. Kahaner, C. Moler, S. Nash, Numerical Methods and Software, Prentice Hall, Englewood Cliffs, NJ, 1989.
[21] C.A. Haynes, H.W. Blanch, J.M. Prausnitz, AICHE J. 39 (1993) 1539.